Digital Camera Identification from Sensor Pattern Noise

Jan Lukáš, Jessica Fridrich, and Miroslav Goljan

Abstract—**In this article, we propose a new method for the problem of digital camera identification from its images based on the sensor's pattern noise. For each camera under investigation, we first determine its reference pattern noise, which serves as a unique identification fingerprint. This is achieved by averaging the noise obtained from multiple images using a denoising filter. To identify the camera from a given image, we consider the reference pattern noise as a spread spectrum watermark, whose presence in the image is established using a correlation detector. Experiments on approximately 320 images taken with 9 consumer digital cameras are used to estimate false alarm rates and false rejection rates. Additionally, we study how the error rates change with common image processing, such as JPEG compression or gamma correction.**

Index Terms—**Fixed pattern noise, sensor identification, digital forensic, pattern noise, pixel non-uniformity**

I. INTRODUCTION

As digital images and video continue to replace their analog counterparts, the importance of reliable, inexpensive, and fast identification of digital image origin will only increase. Reliable identification of the device used to acquire a particular digital image would especially prove useful in the court for establishing the origin of images presented as evidence. In the same manner as bullet scratches allow forensic examiners to match a bullet to a particular barrel with reliability high enough to be accepted in courts, a digital equivalent of bullet scratches should allow reliable matching of a digital image to a sensor. In this paper, we propose to use the sensor pattern noise as the tell-tale "scratches" and show that identification is possible even from processed images.

The problem of digital image authentication may be approached from several different directions. On the most obvious and simplest level, one could inspect the electronic file itself and look for clues in headers or any other attached or associated information. For instance, the EXIF header contains information about the digital camera type and the conditions under which the image was taken (exposure, date and time, etc.). Additional information can be obtained from the quantization table in the JPEG header (some cameras use customized quantization matrices). This header data, however, may not be available if the image is resaved in a different format or recompressed. Another problem is the credibility of information that can be easily replaced.

There has been some effort in the digital watermarking community to embed in the image an invisible fragile watermark (Epson PhotoPC 700/750Z, 800/800Z, 3000Z) or a visible watermark (Kodak DC290), that would carry information about the digital camera, a time stamp, or even biometric of the person taking the image [1]. A similar approach is used in the Canon Data Verification Kit [2] that uses the hash of the image and a special secure memory card to enable tracing the image to a specific Canon camera. Only relatively expensive Canon DSLR cameras (digital single-lens-reflective) support this solution. While the idea to insert the "bullet scratches" in the form of a watermark directly into each image the camera takes is an elegant and empowering solution to the image authentication and camera identification problem, its application is limited to a closed environment, such as "secure cameras" for taking images at crime scenes. Under these controlled conditions, such secure cameras can, indeed, provide a solution to the problem of evidence integrity and origin. This approach, however, cannot solve the problem in its entirety unless all cameras either insert watermarks or embed secure hashes in their images.

Kharrazi et al. [4] proposed a novel idea for camera identification based on supervised learning. In their method, each image is represented using a vector of numerical features extracted from it. Some features are calculated in the spatial domain while the rest are computed in the wavelet domain as in [5]. A multi-class SVM classifier (support vector machine) is then trained to classify images from 5 different cameras. The correct classification ranged from roughly 78% for the worst case to 95% in the best case. Forensic applications at the court are likely to require a substantially higher level of accuracy.

Another previously investigated approach is analysis of

J. Lukáš is a Ph.D. candidate at the Department of ECE, Binghamton University, Binghamton, NY 13902 USA (607-777-5689; fax: 607-777-5689; e-mail: jan.lukas@binghamton.edu).

J. Fridrich is an Associate Professor at the Department of ECE, Binghamton University, Binghamton, NY 13902 USA (607-777-6177; fax: 607-777-4464; e-mail: fridrich@binghamton.edu).

M. Goljan is a Research Scientist at the Department of ECE, Binghamton University, Binghamton, NY 13902 USA (607-777-5793; fax 607-777-4464; e-mail: mgoljan@binghamton.edu).

pixel defects. In [3], the authors show that hot pixels or dead pixels (defective pixels in general), could be used for reliable camera identification even from lossy JPEG compressed images. However, there are cameras that do not contain any defective pixels or cameras that eliminate defective pixels by post-processing their images on-board. For such cameras or sensors, this method cannot be applied.

Kurosawa's approach [6] is the closest in spirit to our method but still fundamentally very different. The authors mention the pattern noise of video-camera imaging sensors for the purpose of camera identification. We note that the *pattern noise* is defined [7] as *any noise component that survives frame averaging*. However, what the authors use in their article is just one component of this noise – the dark current noise (also called *fixed pattern noise*[1] [7]), which is a signal collected from the sensor when it is not exposed to light. Dark current can only be extracted from dark frames. This limits the method because, as the authors themselves point out, camera identification is not possible from regular (non-dark) frames. The fixed pattern noise is only a small component of the pattern noise. Another, and much stronger, component that better survives processing, is the *pixel non-uniformity noise* caused by different sensitivity of pixels to light. The method proposed in this article primarily relies on this component. Another important difference between our approach and [6] is that we use correlation to establish the presence of a certain pattern in an image, while Kurosawa at al. just amplify the *fixed pattern noise* and continue detecting it as local pixel defects.

The camera identification method based on sensor's pattern noise proposed in this paper gives significantly more reliable results compared to previous approaches. Moreover, the origin and character of some components of the pattern noise make it a good candidate for the equivalent of biometrics for sensors ("devicemetrics") suitable for forensic applications.

In the next section, we describe the processing stages inside a digital camera and explain the origin of imperfections and noise sources. In particular, we focus on the properties of the pattern noise. The camera identification algorithm is introduced in Section III, where we also describe the procedure for extracting the reference pattern for each camera and the correlation detector. The performance of the identification method is evaluated using false acceptance and false rejection rates in Section IV, where we report how image processing, such as JPEG compression or gamma correction, influence the error rates. In Section V, we discuss other relevant questions, such as the possibility to remove or forge the pattern noise. The paper is concluded in Section VI.

II.   SIGNAL PROCESSING IN DIGITAL CAMERAS

In this section, we briefly describe the processing stages inside a typical digital camera and discuss various imperfections that inevitably enter the image acquisition process. In particular, we focus on the pattern noise and its

properties and evaluate which components are likely to be useful for camera identification.

The heart of every digital camera is the imaging sensor. The sensor is divided into very small minimal addressable picture elements (pixels) that collect photons and convert them into voltages that are subsequently sampled to a digital signal in an A/D converter. Before the light from the photographed scene reaches the sensor, however, it passes through the camera lenses, an antialiasing (blurring) filter, and then through a color filter array (CFA). The CFA is a mosaic of color filters that block out a certain portion of the spectrum, allowing each pixel to detect only one specific color. The Foveon™ X3 sensor is the only sensor that does not use CFA and is able to capture all three basic colors at every pixel.

If the sensor uses a CFA, the digitized sensor output is further interpolated (demosaicked) using color interpolation algorithms to obtain all three basic colors for each pixel. The resulting signal is then further processed using color correction and white balance adjustment. Additional processing includes gamma correction to adjust for the linear response of the imaging sensor and kernel filtering to visually enhance the image. Finally, the digital image is written to the camera memory device in a user-selected image format. This may require additional processing, such as JPEG compression.

A.   Imperfections and noise

There are numerous sources of imperfections and noise that enter into various stages of the image acquisition process above. Even if the imaging sensor takes a picture of an absolutely evenly lit scene, the resulting digital image will still exhibit small changes in intensity between individual pixels. This is partly because of the *shot noise* (also known as *photonic noise* [7], [8]), which is a random component, and partly because of the *pattern noise* – a deterministic component that stays approximately the same if multiple pictures of the exact same scene are taken. Due to this property, the pattern noise is present in every image the sensor takes and thus can be used for camera identification. Because the pattern noise is a systematic distortion, it may appear that it is improper to call it noise. Nevertheless, by slight abuse of language, the pattern noise is a well established term in the imaging sensor literature [7], [8] and we accept this terminology here as well. We note that averaging multiple images reduces the random components and enhances the pattern noise.

The two main components of the pattern noise are the *fixed pattern noise* (FPN) and the *photo-response non-uniformity noise* (PRNU) (see Fig. 1). The fixed pattern noise (FPN) is caused by dark currents. It primarily refers to pixel-to-pixel differences when the sensor array is *not* exposed to light. Because the FPN is an additive noise, some middle to high-end consumer cameras suppress this noise automatically by subtracting a dark frame [9] from every image they take. FPN also depends on exposure and temperature.

In natural images, the dominant part of the pattern noise is the photo-response non-uniformity noise (PRNU). It is caused primarily by *pixel non-uniformity* (PNU), which is defined as

---

[1] We use the same terminology as Kurosawa et al. [6] and [7], which is, however, different than in [8].

different sensitivity of pixels to light caused by the inhomogenity of silicon wafers and imperfections during the sensor manufacturing process. The character and origin of the PNU noise make it unlikely that even sensors coming from the same wafer would exhibit correlated PNU patterns. As such, the PNU noise is not affected by ambient temperature or humidity.
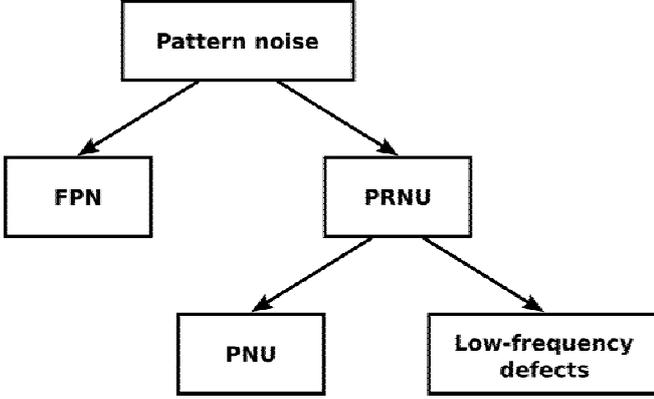
Fig. 1: Pattern noise of imaging sensors.

Light refraction on dust particles and optical surfaces and zoom settings also contribute to the PRNU noise. These components are known as "doughnut" patterns and vignetting and are of low spatial frequency in nature [8]. Because these low frequency components are not a characteristic of the sensor, we should not use them for sensor identification and only use the PNU component, which is an intrinsic characteristic of the sensor.

We now describe a mathematical model of the image acquisition process. Let us denote the photon counts that would be ideally registered by the sensor due to incoming light as $x = (x_{ij})$, $i = 1, \ldots, m, j = 1, \ldots, n$, where $m \times n$ is the sensor resolution Denoting the shot noise as $\eta = (\eta_{ij})$, the additive random noise (represented by read-out noise, etc.) as $\varepsilon = (\varepsilon_{ij})$, and the dark current as $c = (c_{ij})$, the output of the sensor $y = (y_{ij})$ can be expressed in the following form (before any other camera processing)

$$y_{ij} = f_{ij}(x_{ij} + \eta_{ij}) + c_{ij} + \varepsilon_{ij}. \tag{1}$$

The factors f_{ij} are typically very close to 1 and capture the PRNU noise, which is a multiplicative noise. As mentioned above, the signal y goes through a long chain of complex processing before it is stored in an image file. This processing includes operations on a local neighborhood of pixels, such as demosaicking, color correction, or kernel filtering. Some operations may be non-linear in nature, such as gamma correction, white balance, or adaptive color interpolation. Thus, the final pixel values p_{ij}, which we will assume to be in the range $0 \le p_{ij} \le 255$, are

$$p_{ij} = P(y_{ij}, N(y_{ij}), i, j), \tag{2}$$

where P is a non-linear function of y_{ij}, the pixel location (i, j), and values y from a local neighborhood $N(y_{ij})$.

B.   Flat fielding

It is possible to suppress the pattern noise using a process called flat fielding [7], [8], in which the pixel values are first corrected for the additive FPN and then divided by a flat field frame $\hat{f}_{ij}$

$$\hat{x}_{ij} = (y_{ij} - c_{ij}) / \hat{f}_{ij}. \tag{3}$$

In (3), $\hat{x}_{ij}$ is the corrected sensor output and $\hat{f}_{ij}$ is an approximation to f_{ij} obtained by averaging K images of a uniformly lit scene $f_{ij}^{(k)}$, $k = 1, \ldots, K$

$$\hat{f}_{ij} = \frac{\sum_k f_{ij}^{(k)}}{\frac{1}{m \times n} \sum_{i,j,k} f_{ij}^{(k)}}. \tag{4}$$

Note that this process cannot be done correctly from the final pixel values p_{ij} and *must* be performed on the raw sensor output y before any further image processing. While it is commonly done for astronomical imaging[2], consumer digital cameras do not flat-field their images because it is difficult to achieve a uniform sensor illumination inside the camera.

C.   Properties of pixel non-uniformity noise

In order to better understand the impact of the pattern noise on the final image p_{ij} and to determine its properties, we performed the following experiment. Using a light-box producing a uniformly illuminated surface[3], we took 118 images using a Canon G2 camera (for camera specifications, see Table I below). The camera was set to automatic exposure and was focused to infinity. The white balance was set so that the light-box produced neutral gray images.
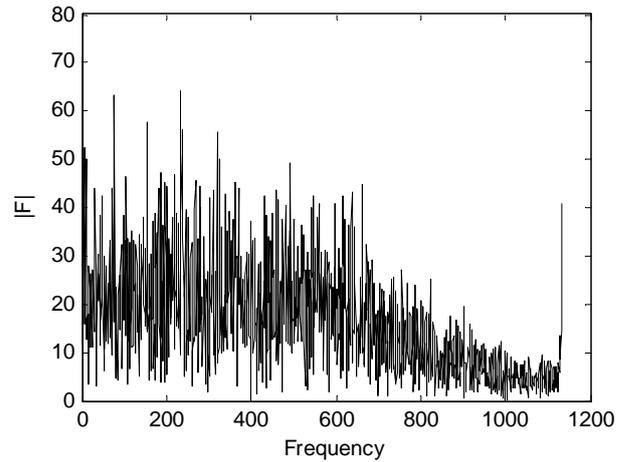
Fig. 2: Magnitude of Fourier transform of one row in an image obtained as average over 118 images of a flat scene.

---

[2] We note that in most scientific applications flat-fielding does not include subtraction of the dark frame because the FPN is usually suppressed by cooling the sensor.

[3] Taking pictures of a flat scene helps reduce the impact of color interpolation and other in-camera processing.

All images exhibited a slight intensity gradient and vignetting. To remove these low-frequency patterns, we applied a high-pass filter with cut-off frequency of $(150/1136)\pi$. After filtering, the images were averaged. The averaging reduced the random noise components, while the pattern noise accumulated. In Fig. 2, we show the magnitude of the Fourier transform F(r) of one pixel row r in the averaged image. The signal r exhibits properties of a white noise signal with an attenuated high frequency band. This attenuation is likely due to the low-pass character of the CFA interpolation algorithm.

The PNU noise can not be present in completely saturated areas of an image, where the pixels were filled to their full capacity, producing a constant signal. It is also clear from (1) that in very dark areas (when $x_{ij} \approx 0$) the amplitude of the PNU noise is suppressed as well, leaving the FPN as the dominant component of the pattern noise.

We close this section with a note that essentially all imaging sensors (CCD, CMOS, JFET, or CMOS-Foveon™ X3) are built from semiconductors and their manufacturing techniques are similar. Therefore, it is reasonable to expect that the pattern noise in all these sensors has similar properties. Although [7] and [8] deal mainly with CCDs, it is noted in [7] (page 92) that CMOS sensors also experience both FPN and PRNU. Moreover, according to [10] the PRNU noise strength is comparable for both CMOS and CCD detectors. As JFET sensors do not differ too much from CMOSs, they should also behave similarly. Our experiments with the CMOS-Foveon™ X3 based Sigma SD9 camera confirm the presence of pattern noise that survives frame averaging and that can be used for camera identification.

III.   CAMERA IDENTIFICATION ALGORITHM

Because of the noise-like character of the PNU noise, it is natural to detect its presence in an image using correlation as is commonly done in robust watermark detection [11]. To verify that a specific image p was taken with camera C, we first determine the camera reference pattern P_C, which is an approximation to the PNU noise. The presence of the reference pattern in p will be established using correlation. We now describe this process in detail.

A.   Camera reference pattern

Because of the complex nature of the processing (2) and because most consumer cameras do not allow access to the raw sensor output y_{ij}, it is generally not possible to extract the PNU noise using flat fielding. It should be, however, possible to obtain an approximation to the PNU noise by averaging multiple images $p^{(k)}$, $k = 1, …, N_p$. This process can be sped up by suppressing the scene content from the image prior to averaging. This is achieved using a denoising filter F and averaging the noise residuals $n^{(k)}$ instead,

$$n^{(k)} = p^{(k)} - F(p^{(k)}). \qquad (5)$$

Another benefit of working with the noise residuals is that the low-frequency components of PRNU are automatically suppressed. Obviously, the larger the number of images N_p, the more we suppress random noise components and the

impact of the scene. Based on our experiments, we recommend using $N_p > 50$.

We have experimented with several denoising filters and eventually decided to use the wavelet-based denoising filter described in Appendix A because it gave us the best results. This is likely because the noise residual obtained using this particular filter contains the least amount of traces of the scene (areas around edges are usually misinterpreted by less sophisticated denoising filters, such as the Wiener filter or the median filter).

Finally, we would like to point out that there are two advantages of this method for obtaining the reference pattern: a) it does not require access to the camera (assuming we have images taken by the camera), b) it is applicable to all cameras independently of the fact whether or not the camera allows access to raw sensor output.

B.   Detection by correlation

To decide whether a specific image p was taken by camera C, we calculate the correlation ρ_C between the noise residual $n = p - F(p)$ and the camera reference pattern P_C

$$\rho_C(p) = corr(n, P_C) = \frac{(n - \overline{n}) \cdot (P_C - \overline{P}_C)}{\|n - \overline{n}\|\|P_C - \overline{P}_C\|}, \qquad (6)$$

where the bar above a symbol denotes the mean value.

We can now experimentally determine the distribution of $\rho_C(q)$ for other images q taken by C and the distribution of $\rho_C(q')$ for images q' that were *not* taken by C. Accepting a parametric model for both distributions, we calculate a threshold using the Neyman-Pearson approach and minimize the false rejection rate (FRR) while imposing a bound[4] on the false acceptance rate (FAR). The value $\rho_C(p)$ is then compared to the threshold to reach the final decision.

To assess the reliability of this camera identification algorithm, in the next section we performed several experiments with 320 images from 9 digital cameras.

IV.   EXPERIMENTS AND RESULTS

In this section, we experimentally estimate the error rates of the camera identification method above. We also study how the error rates are influenced by common image processing operations, such as JPEG compression and gamma correction.

A.   Cameras and test images

For our tests, we prepared an image database containing approximately 320 images from each camera listed in Table I with a variety of outdoor and indoor scenes, including close-ups and landscapes taken under varying light conditions. A few selected images are shown in Appendix B.

Images were taken with and without the flash and with varying zoom settings. Also, these images were taken under vastly different ambient temperatures ranging from winter scenes taken at –10°C to scenes taken at outside temperature

---

[4] This is because in forensic applications in general, it is important to keep the FAR low.

TABLE I
CAMERAS USED IN EXPERIMENTS AND THEIR PROPERTIES.

Camera brand	Sensor	Native resolution	Image format
Canon PowerShot A10	1/2.7-inch CCD	1280×960	JPEG
Canon PowerShot G2	1/1.8-inch CCD	2272×1704	CRW
Canon PowerShot S40	1/1.8-inch CCD	2272×1704	CRW
Kodak DC290	unspecified CCD	1792×1200	TIFF
Olympus Camedia C765 UZ – 1	1/2.5-inch CCD	2288×1712	TIFF
Olympus Camedia C765 UZ – 2	1/2.5-inch CCD	2288×1712	TIFF
Nikon D100	23.7×15.5 mm Nikon DX CCD	3008×2000	NEF
Sigma SD9	20.7×13.8 mm CMOS-Foveon X3	2268×1512	X3F
Olympus Camedia C3030	1/1.8-inch CCD	2048×1536	JPEG

close to 30°C and relative humidity over 90%. Images from Olympus C3030 and Kodak DC290 were taken over a long time span of about 5 years.

We point out that the Canon G2 and S40 share the same CCD sensor type and the two Olympus C765 cameras are of the exact same brand and model.

Table I shows for each camera the imaging sensor, its native resolution, and image format in which the images (all in native resolution if not mentioned otherwise) were taken. Images in the Canon CRW raw format were converted using the Canon Utilities RAW Image Converter version 1.2.1 to the 24-bit true color TIFF format. Images taken in the Nikon NEF raw format were converted by Nikon Capture 4.0 into the 24-bit true color TIFF format. All images from Canon A10 and Olympus Camedia C3030 were collected in the JPEG format. The Sigma SD9 is a semiprofessional DSLR camera with the CMOS-Foveon™ X3 sensor. It only outputs images in its proprietary X3F raw format. All images were converted to 24-bit TIFF using Sigma PhotoPro 2.1.

B.   Experiment I

We calculated the reference pattern for each camera by averaging the noise residual (5) for $N_p = 300$ images from the database. Then, we calculated the correlation of each reference pattern with the noise residual from every image from the database. Unless noted otherwise, when correlating a noise residual with a camera reference pattern of different dimensions, we cropped the larger of the two to fit the dimensions of the smaller one. Because digital cameras differ in image resolution and aspect ratios (3:2 or 4:3), cropping seemed to be the natural choice for comparing *pixel-to-pixel* differences.

For every image from the database of 9×300=2700 images, the correlation with the reference pattern of the camera that took the image was *always* the highest. The distributions were also always well separated indicating that this method for camera identification has good potential. To estimate the FAR and FRR, we performed the following statistical analysis of the experimental data.

The proper way to estimate the FAR and FRR is to collect enough data to experience both types of errors. The Doddington's rule of 30 [14] requires conducting enough tests to experience at least 30 errors. In our case, the distributions of

correlations for the correct camera and all 8 remaining cameras are well separated, which means that we do not observe any errors. Although substantially increasing the number of cameras or test images is the only proper way to estimate the errors, it is not a feasible approach in the short term. Instead, we decided to use a conservative parametric model of the data and obtain estimates of the error rates.

Let $\rho_c^{c'}(i)$, $i = 1, \ldots, N$, denote the vector of $N = 300$ correlations between the reference pattern from camera $c \in \{1, \ldots, 9\}$ with the noise residual from N images from camera c'. Fig. 3 shows an example of the distribution of $\rho_c^{c'}(i)$ for c and c' corresponding to Canon S40 and Olympus C765, respectively. The shape of the distributions changes very much for different combinations of cameras c and c'. In particular, they may have thick tails or may be quite "spiky." We modeled the individual distributions of $\rho_c^{c'}(i)$, $i = 1, \ldots, N$, for fixed c and c' using the Generalized Gaussian model with probability density function

$$f(x;\alpha,\beta,\mu) = \frac{1}{2\alpha\Gamma(1/\beta)} e^{-\left(\frac{|x-\mu|}{\alpha}\right)^{\beta}}. \qquad (7)$$
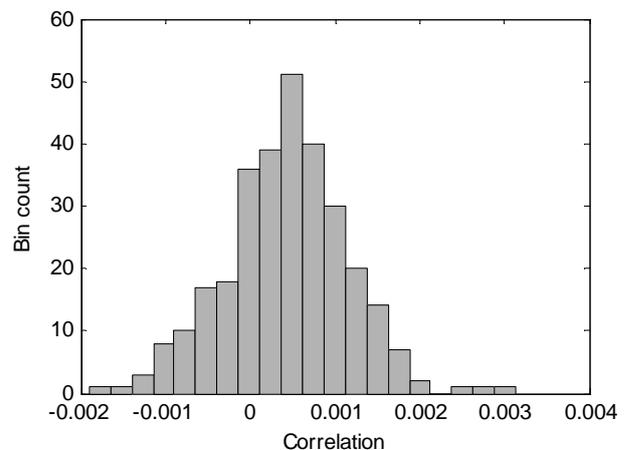
Fig. 3: Distribution of correlation of the reference pattern from Canon S40 with noise residual from 300 Olympus C765 images.

The parameters were estimated using the method of moments [15]. In particular, given a vector of correlations $\rho(i)$, $i = 1, \ldots, N$,

$$\hat{\mu} = \frac{1}{N} \sum_{i=1}^{N} \rho(i),$$

$$\hat{\beta} = G^{-1}(\hat{m}_1^2 / \hat{m}_2), \tag{8}$$

$$\hat{\alpha} = \hat{m}_1 \frac{\Gamma(1/\hat{\beta})}{\Gamma(2/\hat{\beta})},$$

where

$$\hat{m}_1 = \frac{1}{N} \sum_{i=1}^{N} |\rho(i) - \hat{\mu}|,$$

$$\hat{m}_2 = \frac{1}{N} \sum_{i=1}^{N} |\rho(i) - \hat{\mu}|^2, \tag{9}$$

$$G(x) = \frac{[\Gamma(2/x)]^2}{\Gamma(1/x)\Gamma(3/x)},$$

and $\Gamma(x)$ is the Gamma function.

The generalized Gaussian model was used intentionally because models that allow thicker tails will lead to more conservative error estimates. In Fig. 4, we show an example of the distribution of correlations between the reference pattern from Olympus C3030 and noise residual from Canon G2 and the corresponding generalized Gaussian model fit.
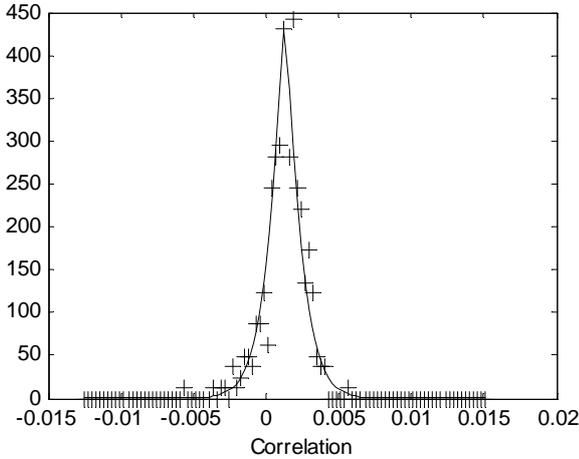
Fig. 4: Distribution of correlation (plus signs) and its generalized Gaussian fit (line) with the shape parameter $\beta = 1.173$.

We could estimate the FAR and the FRR for each camera c by fitting the model to the distribution of $\rho_c^c(i)$, $i = 1, \ldots, N$, and modeling $\rho_c^{c'}(i)$, $i = 1, \ldots, N$, for *all* cameras $c' \neq c$ as one signal. However, when pooling the correlations $\rho_c^{c'}(i)$ for all cameras $c \neq c'$, the resulting distribution may be multi-modal (see Fig. 5). This is because the reference patterns of some cameras exhibit a small positive correlation (e.g., Canon S40, Canon G2, and Nikon D100). We hypothesize that this small correlation is due to similar in-camera processing, such as the same CFA interpolation algorithm. Consequently, although

the distributions of $\rho_c^{c'}(i)$ for individual pairs of c and c' are well modeled using the generalized Gaussian, when pooled together, they no longer follow the model. Therefore, we carried out the error analysis in the following manner.

Let $F_c^{c'}$, $1 \leq c, c' \leq 9$, be the cumulative density function of the generalized Gaussian distribution (7) with parameters (α, β, μ) determined from correlations $\rho_c^{c'}(i)$, $i = 1, \ldots, N_p$, between the reference pattern of the c-th camera and the noise residual of $N = 300$ images taken by camera c'. To decide whether camera c_0 took a given image p, we calculate the correlation ρ between the noise residual of p and the reference pattern of camera c_0 and compare to a threshold t for this camera. If $\rho > t$, we will conclude that p was taken with camera c_0. In forensic applications, it is important to minimize the probability of false acceptance. Thus, we use the Neyman-Pearson approach and determine the value of t by maximizing the probability of detection (or, equivalently minimizing the FRR) given an upper bound on the FAR, FAR $< \alpha_{\text{FAR}}$.
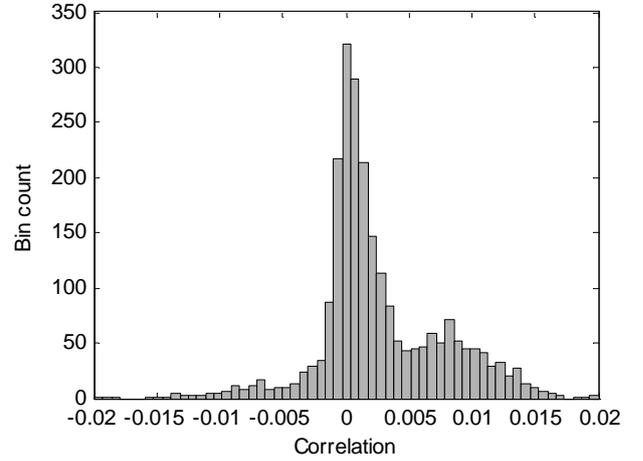
Fig. 5: Distribution of correlation of the reference pattern from Nikon D100 with noise residual from approx. 8×300 images from all other cameras.

For a given threshold t, the probability of false rejection is

$$\text{FRR} = F_{c_0}^{c_0}(t). \tag{10}$$

Assuming p was not taken by camera c_0 but is classified as coming from c_0 based on threshold t, we obtain

$$\text{FAR} = 1 - \prod_{\substack{c=1 \\ c \neq c_0}}^{9} F_{c_0}^c(t). \tag{11}$$

Thus, the FRR will be minimized for the largest t that satisfies

$$1 - \prod_{\substack{c=1 \\ c \neq c_0}}^{9} F_{c_0}^c(t) \leq \alpha_{\text{FAR}}. \tag{12}$$

TABLE II
DECISION THRESHOLD t AND FRR FOR ALL 9 DIGITAL CAMERAS FOR FAR $= 10^{-3}$.

Processing Camera	none		Gamma 0.7		Gamma 1.4	
	t	FRR	t	FRR	t	FRR
Nikon	0.0449	4.68×10^{-3}	0.0443	1.09×10^{-2}	0.0435	6.33×10^{-3}
C765 - 1	0.0170	3.79×10^{-4}	0.0163	3.88×10^{-4}	0.0172	3.85×10^{-4}
C765 - 2	0.0080	5.75×10^{-11}	0.0076	2.57×10^{-11}	0.0081	2.83×10^{-10}
G2	0.0297	2.31×10^{-4}	0.0271	3.23×10^{-4}	0.0313	4.78×10^{-5}
S40	0.0322	1.42×10^{-4}	0.0298	1.64×10^{-4}	0.0343	1.02×10^{-4}
Sigma	0.0063	2.73×10^{-4}	0.0060	2.93×10^{-4}	0.0064	2.76×10^{-4}
Kodak	0.0097	1.14×10^{-11}	0.0096	1.08×10^{-8}	0.0094	3.73×10^{-13}
C3030	0.0209	1.87×10^{-3}	0.0216	1.58×10^{-3}	0.0195	2.67×10^{-3}
A10	0.0166	7.59×10^{-5}	0.0162	4.71×10^{-5}	0.0160	2.93×10^{-4}

Processing Camera	JPEG 90		JPEG 70		JPEG 50	
	t	FRR	t	FRR	t	FRR
Nikon	0.0225	3.71×10^{-3}	0.0231	5.83×10^{-2}	0.0210	1.63×10^{-1}
C765 - 1	0.0122	5.36×10^{-6}	0.0064	1.55×10^{-6}	0.0060	1.17×10^{-4}
C765 - 2	0.0061	0	0.0065	9.63×10^{-14}	0.0065	2.14×10^{-6}
G2	0.0097	8.99×10^{-11}	0.0079	4.85×10^{-11}	0.0076	5.13×10^{-4}
S40	0.0133	3.96×10^{-11}	0.0085	4.41×10^{-14}	0.0083	9.48×10^{-5}
Sigma	0.0050	3.44×10^{-6}	0.0055	9.16×10^{-6}	0.0059	6.57×10^{-5}
Kodak	0.0107	2.27×10^{-9}	0.0127	4.53×10^{-4}	0.0131	4.65×10^{-3}

Because (11) is monotonically decreasing with t, we find the threshold t by solving (12) where we replace the inequality sign with equality. In each particular case, this equation must be solved numerically. Once the threshold is found, the FRR is determined from (10).

The first two columns in Table II show the FRR for all 9 cameras when the decision threshold was set to obtain FAR $= 10^{-3}$. We point out that it is possible to distinguish between the two Olympus C765 cameras of the exact same brand and model. This supports our choice of the PNU noise as "biometrics" for sensors.

The identification is successful for Canon A10 and Olympus C3030, although their images were only available as JPEGs and their reference patterns were also calculated from JPEG images rather than uncompressed TIFF images.

Also note in Table II that reliable camera identification is possible for the Sigma SD9 camera equipped with a CMOS sensor.

Table II indicates that the camera identification is the least reliable for Nikon D100. This is because the distribution of correlations between the Nikon reference pattern with noise residuals from other cameras has thicker tails than for other cameras (e.g., the shape parameter $\beta = 0.78$ for images from Canon A10). This increases the FRR. We hypothesize that the reason for this is the physical size of pixels. Semi-professional DSLR sensors have larger physical dimensions than those in compact digital cameras and thus larger pixels. Therefore, the PNU noise will be less pronounced due to averaging material inhomogenities over a larger area and more robust manufacturing, while random noise components are more likely to increase.

C. *Experiment II (gamma correction)*

Digital images are often subjected to point-wise operations, such as brightness/contrast adjustment or gamma correction.

Because most spread spectrum watermarks [11] are fairly insensitive to such operations, the camera identification procedure is expected to be fairly robust to gamma adjustment, as well.

We repeated Experiment I after processing images from all cameras using gamma correction with $\gamma = 0.7$ and 1.4. These two values were chosen as the minimal and maximal gamma values that one can typically encounter in practice. JPEG images from Canon A10 and Olympus C3030 cameras were converted to bitmaps first and then gamma corrected.

The results in terms of FRR are shown in Table II in corresponding columns. The results confirm our expectations that gamma correction has little influence on the reliability of camera identification.

D. *Experiment III (JPEG compression)*

Because it is likely that in practice images will be stored in the lossy JPEG format, in this section we investigate the impact of JPEG compression on the reliability of camera identification.

In Experiment I, all images from Canon A10 and Olympus C3030 were already taken in the JPEG format (JPEG quality factor approximately 93–97 for Canon A10 and 70–95 for Olympus C3030). This indicates that the identification method is robust to JPEG compression. We decided to verify this claim for the remaining 7 cameras under more controlled conditions. We repeated Experiment I after saving all 7×300 images as JPEGs with quality factors 50, 70, and 90.[5]

In Table II, we show the FRR for a fixed FAR $= 10^{-3}$ for JPEG quality factors 90, 70, and 50. For quality factor 90, we can see that, with the exception of Kodak DC290, the FRRs decreased when compared to the results obtained for raw

---

[5] Reference patterns were obtained from raw images as before.

images (the first two columns in Table II). We now attempt to explain this somewhat surprising result.

Although JPEG compression does decrease the average value of correlations between the image noise residual and the correct reference pattern, it does so very gradually with the decreasing quality factor. However, we observed that JPEG compression with quality factor 90 or less almost completely suppresses the small positive correlations between the reference patterns that can be seen in Fig. 5 (compare with Fig. 6). Additionally, JPEG compression makes the tails of the distributions $\rho_c^{c'}(i)$, for $c \neq c'$ somewhat thinner. The combined effect of both phenomena results in more reliable identification.
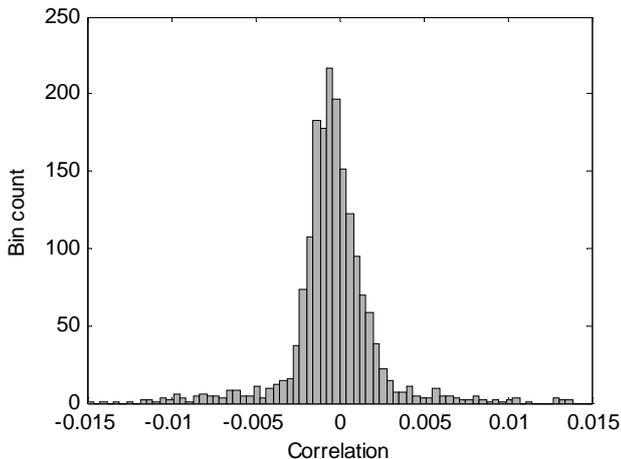
Fig. 6: Distribution of correlation of the reference pattern from Nikon D100 with noise residual from approximately 6×300 JPEG compressed images with quality factor 90 from six other cameras.

E.   Experiment IV (resampling and JPEG compression)

Most digital cameras have an option to save images at lower resolutions than the maximal resolution supported by their sensor. In this section, we report some preliminary results of our investigation whether or not it is possible to identify images already taken at a lower resolution. We note that it is not possible to simulate the resizing off line on a computer without a detailed knowledge of how each camera produces images of smaller resolution. Because this information is considered proprietary by most camera manufacturers, we had to prepare a new test database of images already taken at lower resolution. For this reason, we limited this investigation to just one camera – Canon G2.

We set the camera to take images at a lower resolution of 1600×1200 and took 84 test images. Total of 28 images were taken at low-quality setting (average JPEG quality factor of 72), while the remaining 56 images were taken at the highest-quality setting (with average quality factor 97). We now wish to decide which of the 9 cameras in our tests most likely took the images.

Let us assume for simplicity that we know that the images were taken at a lower resolution or were rescaled on a computer, but have not been cropped. This assumption rules out cameras with the 3:2 image aspect ratio (Nikon D100,

Sigma SD9, and Kodak DC290). For the remaining 6 cameras, we simply resampled[6] each noise residual to the native resolution of each camera and then computed the correlation with its reference pattern.

Due to the small number of images, we did not analyze the results statistically as in the previous sections. Instead, we only include in Fig. 7 a scatter plot of correlation values between the noise residual from all 84 images with all 6 reference patterns. We see that the correlation with Canon G2 camera was always the highest even for the low-quality JPEGs (images 6–33).

We note that a much more extensive experiment performed on more images and across all cameras is necessary to determine the error rates of camera identification from low-resolution images. This preliminary result is, nevertheless, encouraging.
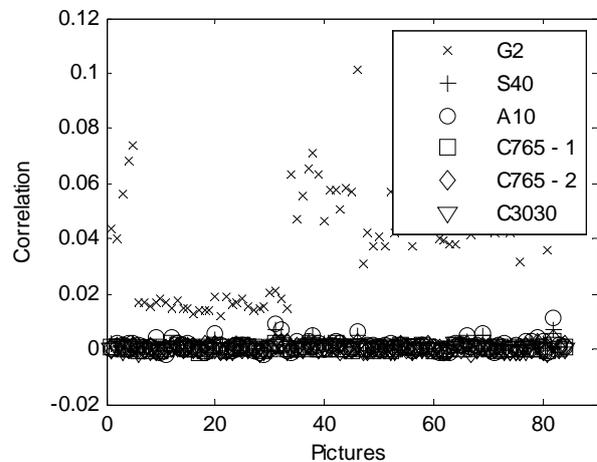
Fig. 7: Correlation of noise residuals from 84 Canon G2 1600×1200 JPEG images with 6 reference patterns.

F.   Experiment V (stability of pattern noise over time)

If the pattern noise is to be used for forensic camera identification, it must be stable over a wide range of environmental conditions, camera settings (zoom, ISO, etc.), and over time. Since our image databases contained images taken under widely varying environmental conditions, different zoom and ISO settings, and battery status, the results of Section IV indicate that the pattern noise is fairly stable. However, all test images were taken over a relatively short period of time of 1–2 years. The stability of the camera identification algorithm over time is the subject of this section.

TABLE III
AVERAGE CORRELATION OVER TIME.

Year	2000	2001	2002	2003	2004	2005
Correlation	0.055	0.044	0.056	0.047	0.047	0.053

We narrowed this experiment to the Kodak DC 290 camera because this was the only camera for which we had images taken over a span of many years (2000–2005). All images were taken at full resolution 1200×1792 in the JPEG format

---

[6] Bicubic resampling was used in all experiments.

("better quality" as defined in camera specifications). The number of images ranged from 56 for year 2001 to more than 700 for year 2003. For each year, we computed the average correlation with the reference pattern obtained from pictures taken in the first quarter of 2004. Table III indicates that the average correlation value varies very little over time.

V. FORGING AND MALICIOUS PROCESSING

Since camera identification techniques are likely to be used in the court, we need to address malicious attacks intended to fool the identification algorithm, such as intentionally removing the pattern noise from an image to prevent identification or extracting the noise and copying it to another image to make it appear as if the image was taken with a particular camera.

We distinguish two situations: 1) the attacker is informed and has either the camera or many images taken by the camera or 2) the attacker is uninformed in the sense that he only has access to one image.

We first discuss the issue of removing the pattern noise or preventing its successful detection. As already noted in Section II.B, an informed attacker can suppress the pattern noise by dark frame subtraction and flat-fielding. However, images are not typically stored in raw formats and are only available as TIFF/JPEG, which means they are already processed in the camera (Eq. (2) in Section II). As a result, it is in general not possible to perform flat fielding correctly from a TIFF/JPEG image.

A simpler way to remove the pattern noise P_C, well-known to researchers working in robust watermarking, is as follows. The attacker can arrange for $\rho_C = 0$ for any image p taken with C by solving the equation $corr(p+\alpha P_C, P_C) = 0$ with respect to α and taking $p+\alpha P_C$ as the forged image.

An uninformed attacker could attempt to remove the pattern noise by applying the same denoising filter. While this, indeed, decreases the correlation value with the correct pattern approximately by a factor of two, in most cases correct identification will still be possible. However, repetitive application of the filter or more aggressive denoising filters will likely prevent correct identification.

The easiest way to prevent a simple detection of the reference pattern is desynchronization, such as slight rotation, possibly combined with other processing that might include resizing, cropping, and filtering. Probably the simplest *active* measure that the photographer can use to complicate image identification later is to take images using a continuous digital zoom, a feature that many consumer digital cameras have today.

The second problem we now investigate is whether it is possible to make an arbitrary image look as if it was taken by a specific camera. Again, having access to the reference pattern or the camera makes this indeed possible. We denoised 20 Canon G2 pictures and added to them the reference pattern from Canon S40. We increased the amplitude of the added noise, till we reached a correlation that was higher than the correlation the image previously had with the Canon G2

reference pattern. The peak signal to noise ratio (PSNR) for the forged images was on average 37.5dB and the images were visually indistinguishable from originals. The forgeries still had higher correlations with the Canon G2 reference pattern than expected from different camera images, but this correlation could be eliminated using some of the techniques mentioned above.

We also tried to plant the noise extracted from a single Canon S40 image using the denoising filter [12] into a denoised Canon G2 image. The correlation of the noise extracted from the resulting image with the Canon S40 reference pattern was usually within the range of the typical correlation values achieved by other Canon S40 images. This kind of malicious processing requires multiplying the added noise with a perceptual mask [11] to avoid creating visible artifacts.

Overall, we conclude that malicious manipulation that will fool the identification algorithm is, indeed, possible if the attacker possesses enough skill in signal processing. We note that it is unlikely that there exists a numerical identification characteristic computed from digital images that could not be compromised by a sufficiently sophisticated opponent. All previously proposed techniques based on defective pixels [3] [6] or image features [4], are certainly vulnerable to malicious attacks as well.

VI. CONCLUSIONS

We have developed a new approach to the problem of camera identification from images. Our identification method uses the pixel non-uniformity noise which is a stochastic component of the pattern noise common to all digital imaging sensors (CCD, CMOS, including Foveon™ X3, and JFET). The presence of this noise is established using correlation as in detection of spread spectrum watermarks. We investigated the reliability of camera identification from images processed using JPEG compression, gamma correction, and a combination of JPEG compression and in-camera resampling. Experimental results were evaluated using FAR and FRR error rates. We note that the proposed method was successful in distinguishing between two cameras of the same brand and model.

Since the identification technique requires proper synchronization, geometrical operations, such as cropping, resizing, rotation, digital zoom, cause desynchronization and prevent correct camera identification. In this case, the detection algorithm will have to resort to brute force searches. Techniques, such as the one described in [16], may help us alleviate the computational complexity of brute force searches by retrieving some information about applied geometrical operations. The searches will, however, inevitably increase the FAR.

We would like to point out that the problem of camera identification should be approached from multiple directions, combining the evidence from other methods, such as the feature-based identification [4], which is less likely to be influenced by geometrical transformations.

Our future plans include developing methods for detection

of digital forgeries by detecting the presence of the pattern noise in disjoint regions. Finally, we plan to extend this technique to identification of video-cameras and scanners.

REFERENCES

[1] Blythe, P. and Fridrich, J.: "Secure Digital Camera," *Digital Forensic Research Workshop*, Baltimore, August 11–13, 2004.

[2] "Canon Data Verification Kit DVK-E2," available: http://www.dpreview.com/news/0401/04012903canondvke2.asp .

[3] Geradts, Z., Bijhold, J., Kieft, M., Kurosawa, K., Kuroki, K., and Saitoh, N.: "Methods for Identification of Images Acquired with Digital Cameras," *Proc. of SPIE, Enabling Technologies for Law Enforcement and Security*, vol. 4232, pp. 505–512, February 2001.

[4] Kharrazi, M., Sencar, H. T., and Memon, N.: "Blind Source Camera Identification," *Proc. ICIP' 04*, Singapore, October 24–27, 2004.

[5] Farid, H. and Lyu, S.: "Detecting Hidden Messages Using Higher-Order Statistics and Support Vector Machines," in F.A.P. Petitcolas (ed.): *5th International Workshop on Information Hiding, LNCS* vol. 2578, Springer-Verlag, Berlin-Heidelberg, New York, pp. 340–354, 2002.

[6] Kurosawa, K., Kuroki, K., and Saitoh, N.: "CCD Fingerprint Method - Identification of a Video Camera from Videotaped Images," *Proc of ICIP' 99*, Kobe, Japan, pp. 537–540, October 1999.

[7] Holst, G. C.: *CCD Arrays, Cameras, and Displays*, 2nd edition, JCD Publishing & SPIE Pres, USA, 1998.

[8] Janesick, J. R.: *Scientific Charge-Coupled Devices*, SPIE PRESS Monograph vol. PM83, SPIE–The International Society for Optical Engineering, January, 2001.

[9] "Dark Frame Subtraction," *Qimage help*, available: http://www.ddisoftware.com/qimage/qimagehlp/dark.htm.

[10] Janesick, J. R.: "Dueling Detectors", *OE Magazine*, vol. 2(2), February 2002.

[11] Cox, I., Miller, M.L., and Bloom, J.A.: *Digital Watermarking*, Morgan Kaufmann, San Francisco, 2001.

[12] Mihcak M.K., Kozintsev, I., and Ramchandran, K.: "Spatially adaptive statistical modeling of wavelet image coefficients and its application to denoising," in *Proc. IEEE Int. Conf. Acoustics, Speech, and Signal Processing*, Phoenix, AZ, Mar. 1999, vol. 6, pp. 3253–3256.

[13] Donoho, D., Duncan, M. R., Huo, X., and Levi, O.: *Wavelab 802*, available: http://www-stat.stanford.edu/~wavelab/ .

[14] Doddington, G., Liggett, W., Martin, A., Przybocki, M., and Reynolds, D.: "Sheep, Goats, Lambs and Wolves: A Statistical Analysis of Speaker Performance in the NIST 1998 Speaker Recognition Evaluation," in *Proceedings of 5th International Conference of Spoken Language Processing*, ICSLP 98, Sydney, Australia. Paper 608 on CD-ROM.

[15] Meignen, S. and Meignen, H.: "On the Modeling of DCT and Subband Image Data for Compression," *IEEE Trans. on Image Processing*, vol. 4, pp. 186–193, 1995.

[16] Popescu, A.C. and Farid H.: "Statistical Tools for Digital Forensic," in J. Fridrich (ed.): *6th International Workshop on Information Hiding, LNCS* vol. 3200, Springer-Verlag, Berlin-Heidelberg, New York, pp. 128–147, 2004.

APPENDIX A (DENOISING FILTER)

Our implementation of the denoising filter is based on the work proposed in [12]. It is constructed in the wavelet domain using the Wavelab package [13]. Let us assume that the image is a grayscale 512×512 image. Larger images can be processed by blocks and color images are denoised for each color channel separately. The high-frequency wavelet coefficients of the noisy image are modeled as an additive mixture of a locally stationary i.i.d. signal with zero mean (the noise-free image) and a stationary white Gaussian noise $N(0, \sigma_0^2)$ (the noise component). The denoising filter is built in two stages. In the first stage, we estimate the local image variance, while in the second stage the local Wiener filter is used to obtain an estimate of the denoised image in the wavelet domain. We now describe the individual steps:

Step 1. Calculate the fourth-level wavelet decomposition of the noisy image with the 8-tap Daubechies QMF. We describe the procedure for one fixed level (it is executed for the high-frequency bands for all four levels). Denote the vertical, horizontal, and diagonal subbands as $h(i,j)$, $v(i,j)$, $d(i,j)$, where (i,j) runs through an index set J that depends on the decomposition level.

Step 2. In each subband, estimate the local variance of the original noise-free image for each wavelet coefficient using the MAP estimation for 4 sizes of a square $W \times W$ neighborhood N, for $W \in \{3, 5, 7, 9\}$.

$$\hat{\sigma}_W^2(i,j) = \max\left(0, \frac{1}{W^2} \sum_{(i,j) \in N} h^2(i,j) - \sigma_0^2\right), (i,j) \in J.$$

Take the minimum of the 4 variances as the final estimate,

$$\hat{\sigma}^2(i,j) = \min\left(\sigma_3^2(i,j), \sigma_5^2(i,j), \sigma_7^2(i,j), \sigma_9^2(i,j)\right), (i,j) \in J.$$

Step 3. The denoised wavelet coefficients are obtained using the Wiener filter

$$h_{\text{den}}(i,j) = h(i,j) \frac{\hat{\sigma}^2(i,j)}{\hat{\sigma}^2(i,j) + \sigma_0^2}$$

and similarly for $v(i,j)$, and $d(i,j)$, $(i,j) \in J$.

Step 4. Repeat Steps 1–3 for each level and each color channel. The denoised image is obtained by applying the inverse wavelet transform to the denoised wavelet coefficients.

To complete the description of the denoising filter, we now briefly discuss the choice of the parameter σ_0 by investigating how the correlations between noise residuals and reference patterns are influenced when setting σ_0 to different values. We used the reference pattern for the Canon G2 camera obtained in Section II.C by averaging 118 uniform gray images. Note that we do not need the filter for this. Using the filter with parameter $\sigma_0 \in \{1, \ldots, 6\}$, we calculated the noise residual for 20 images from each camera (20×9=180 images total). Then, we computed the correlations between the G2 reference pattern above and the noise residual from all 180 images. Fig. 8 shows the correlations averaged over all 20 images for each camera as a function of σ_0. This figure shows that the dependence of the correlations on σ_0 is relatively flat (the small positive bias between G2 and S40 is commented upon in Section II.B.).

In all experiments, we used $\sigma_0 = 5$ (for dynamic range of images 0, ..., 255) to be conservative and to make sure that the filter extracts substantial part of the PNU noise even for cameras with a large noise component.
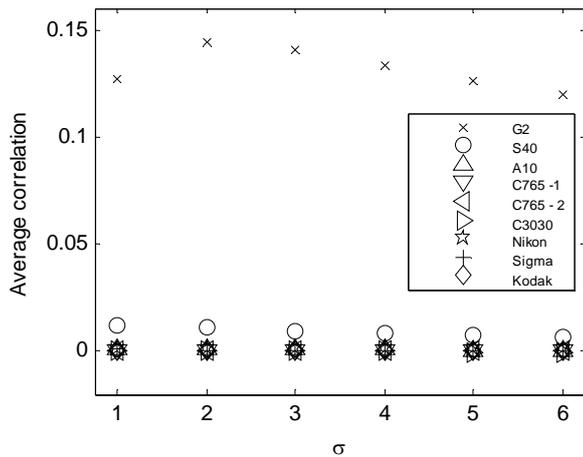
Fig. 8: Correlation between the G2 reference pattern and the noise component from images from other cameras obtained using the denoising filter with parameter σ.

APPENDIX B

A few sample images used in our experiments:

Jan Lukáš has received his MS in Applied Mathematics from Czech Technical University in Prague in 1998.

He is a Ph.D. Candidate at the Dept. of Electrical and Computer Engineering at Binghamton University (SUNY). His main reasearch interests are in Digital Image Forensic, Digital Image Authentication and Digital Forgeries Detection.

Mr. Lukáš's research work has been already appreciated by Best Student Paper Award at Image & Video Communications and Processing 2005 (part of SPIE Electronic Imaging 2005) and by Graduate Student Excellence in Research Award at Binghamton University in spring 2006.

Jessica Fridrich holds the position of Associate Professor at the Dept. of Electrical and Computer Engineering at Binghamton University (SUNY).

She has received her PhD in Systems Science from Binghamton University in 1995 and MS in Applied Mathematics from Czech Technical University in Prague in 1987. Her main interests are in Steganography, Steganalysis, Digital Watermarking, and Digital Image Forensic.

Dr. Fridrich's research work has been generously supported by the US Air Force. Since 1995, she received 18 research grants totaling over $5mil for projects on data embedding and steganalysis that lead to more than 80 papers and 7 US patents. Dr. Fridrich is a member of IEEE and ACM.

Miroslav Goljan received the M.S. degree in mathematical informatics from Charles University in Prague, Czech Republic, in 1984 and the Ph.D. in electrical engineering from Binghamton University, State University of New York, in 2002.

He is a Research Scientist at the Department of Electrical and Computer Engineering, Binghamton University. His research focuses on steganography, steganalysis, reversible data hiding and watermarking, and digital media authentication.